Role of hydrogen bonding in charge-ordered organic conductor α-(BEDT-TTF)$_2$I$_3$ probed by ^{127}I nuclear quadrupole resonance

T. Kobayashi [1,2,3,*] Y. Kato,[1] H. Taniguchi [1] T. Tsumuraya [4] K. Hiraki,[5] and S. Fujiyama [3]

[1]*Graduate School of Science and Engineering, Saitama University, Saitama 338-8570, Japan*
[2]*Research and Development Bureau, Saitama University, Saitama 338-8570, Japan*
[3]*Meson Science Laboratory, RIKEN, Saitama 351-0198, Japan*
[4]*Magnesium Research Center, Kumamoto University, Kumamoto 860-8555, Japan*
[5]*Center for Integrated Science and Humanities, Fukushima Medical University, Fukushima 960-1295, Japan*

We present ^{127}I nuclear quadrupole resonance spectra and nuclear relaxation of α-(BEDT-TTF)$_2$I$_3$ that undergoes a charge-ordering transition. Only one of the two I$_3$ anion sites shows a significant differentiation in the electric field gradients across the first-order transition. The charge modulation only in the BEDT-TTF layers cannot reproduce; instead, an anion-donor interaction accompanied by hydrogen bonding is necessary. The dominating source for the nuclear relaxation is the local libration of the I$_3$ anions, but an anomalous peak is detected just below the transition, as observed by ^{13}C NMR.

I. INTRODUCTION

Electronic correlation in a quasi-two-dimensional organic conductor (BEDT-TTF)$_2$$X$ stabilizes various ground states, including quantum spin liquids or Dirac electron systems. Molecular arrangements of the BEDT-TTF [bis(ethylenedithio)tetrathiafulvalene, hereafter abbreviated as ET] in the alternating conducting planes specify the electronic correlation leading to various physical properties [1,2]. Of these, α, β'', or θ type molecular arrangements establish two-dimensional 3/4-filled (1/4-filled hole) electronic bands. Long-range Coulomb interactions cause ground states such as charge ordering (CO), ferroelectricity [3,4], charge glass [5], and superconductivity [6–9].

A quasi-two-dimensional organic conductor α-ET$_2$I$_3$, shown in Fig. 1(a), is one of the most studied organic conductors [10]. This material has a quarter-filled electronic band, showing a Mott-insulating instability. One prominent property of α-ET$_2$I$_3$ is the realization of a Dirac electron system under applied pressure [11–15]. At ambient pressure, the system shows a metal-insulator transition at $T_{\mathrm{CO}} \approx 135$ K associated with the CO transition [3,4,16]. It is widely accepted that the modulation pattern of the CO is not checkerboardlike but zigzag-chain-like with charge-rich sites A and B, and charge-poor sites A$'$ and C [Fig. 1(b)], as revealed by x-ray structural analysis [17], infrared and Raman spectroscopies [18–20], and ^{13}C-NMR spectroscopy [21–24].

Despite the consensus on the modulation pattern, issues remain regarding the mechanism of the CO transition. Many theoretical studies have been conducted and a variety of proposals have been made. Coulomb repulsion in the quarter-filled band of the ET layers has been proposed [1,26–29], followed by a claim that the electron-phonon interaction plays

a crucial role to reproduce the CO pattern [30–33]. While these theories consider only interactions within the intra-ET layers, some approaches actively incorporate the role of the anion layer through hydrogen bonding. Reference [34] pointed out the significant role of the H-I$^{-1/2}$ σ bond between the anion and edge protons in the ET molecule. Since the energy difference between the σ bond and π electrons of donor molecules are far apart, the σ hybridization is expected to conserve the total charge density in the ET layers. However, the σ bond can constrain atomic positions across the structural phase transition, and also the problem regarding the stability of the Mottness of the quarter-filled band perturbed by the hydrogen bond attracts much attention.

In this paper, we propose ^{127}I-nuclear quadrupole resonance (NQR) as a microscopic tool to examine the specific H-I$^{-1/2}$ bonds. The NQR spectra of α-ET$_2$I$_3$ are qualitatively reproduced using first-principles calculations, which enables us to claim the microscopic interactions that occur during the CO transition. Utilizing another merit of NQR, unlike with ^{13}C NMR, we can directly observe static and dynamic charge properties via an electric field gradient (EFG), and we found the zigzaglike charge modulation in the CO state across a first-order transition. Only one of two I-spectral lines shows significant splitting at T_{CO}, which cannot be reproduced by an electrostatic interaction only from the ET layers, and an interaction between the ET and I$_3$ layers through such a hydrogen bonding is necessary. The nuclear spin-lattice relaxation rate $(1/T_1)$ is dominated by local fluctuation of the I$_3$ anions, of which the energy is five times smaller than the Debye frequency. We also found enhancements of $1/T_1$ just below T_{CO}.

II. EXPERIMENTS

Single crystals of α-ET$_2$I$_3$ were grown by the standard electrochemical reaction [16]. The ^{127}I-NQR experiment was performed on a polycrystalline sample of 14.2 mg under
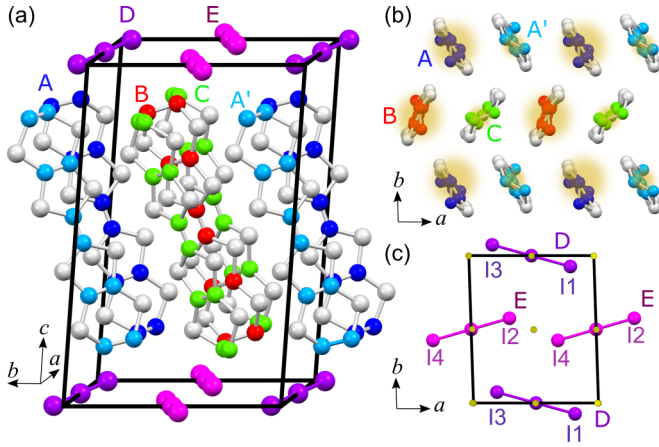
*tkobayashi@mail.saitama-u.ac.jp

FIG. 1. Crystal structure of (a) α-I$_3$ [25]. BEDT-TTF molecules labeled as A, B (A', C) show charge-rich (charge-poor) sites for $T < T_{CO}$. (b) Top view of the conduction plane in the CO state. (c) Insulating I$_3$ plane. The inversion center is lost for $T < T_{CO}$, by which I1 and I3, and I2 and I4 sites become crystallographically inequivalent.

FIG. 2. (a) Temperature evolution of the ^{127}I-NQR spectra. The inset shows the central peak at 6 K. (b) Temperature dependence of the ^{127}I-NQR frequency. The solid lines are the fitting curves of $\nu_Q(T) = \nu_0(1 - \alpha T^{3/2})$.

zero magnetic fields. The NQR spectrum was obtained by fast Fourier transformation of the spin-echo signal with a $\pi/2$-π pulse sequence, where the typical $\pi/2$ pulse length was 2.5 μs. The $1/T_1$ were measured using the inversion and saturation recovery methods and were obtained by fitting the magnetization curves using

$$1 - \frac{M(t)}{M(\infty)} \propto \frac{3}{28} \exp\left(-\frac{3t}{T_1}\right) + \frac{25}{28} \exp\left(-\frac{10t}{T_1}\right) \quad (1)$$

(see the Supplemental Material [35] and also Refs. [36,37] therein). Here, t is the interval between inversion (saturation) and the first $\pi/2$ pulses, and $M(t)$ is the magnetization at time t. We confirmed that the same T_1 values were obtained by both methods in the appropriate temperature range. EFGs at the iodine sites of α-ET$_2$I$_3$ were calculated using the first-principles calculations based on the full-potential linearized augmented plane-wave (FLAPW) method [38,39]. The calculations are based on density-functional theory (DFT), and the exchange and correlation potential is represented by a generalized gradient approximation in the Perdew-Burke-Ernzerhof formula [35,40].

III. RESULTS AND DISCUSSION

A. NQR spectra

We found two ^{127}I-NQR spectral lines at 172.2 and 173.1 MHz at 150 K, as shown in Fig. 2(a), while sweeping in the range of 170–176 MHz. Reported ^{127}I-NQR studies of I$_3$ anions in quaternary ammonium salts indicated that the observed resonances are ascribed to $\pm 1/2 \leftrightarrow \pm 3/2$ transitions of the terminal iodines [41,42]. At a terminal iodine, the EFG tensor is nearly axially symmetric [42] [i.e., $\eta = (V_{xx} - V_{yy})/V_{zz} \simeq 0$, where V_{ii} ($i = x, y, z$) are the diagonal components of the EFG tensor]. The NQR frequency ν_Q is expressed as $\nu_Q = \frac{3eQV_{zz}}{20h}(1 + \frac{59}{54}\eta^2)$, where e, Q, and h are the elementary charge, the nuclear quadrupole moment of
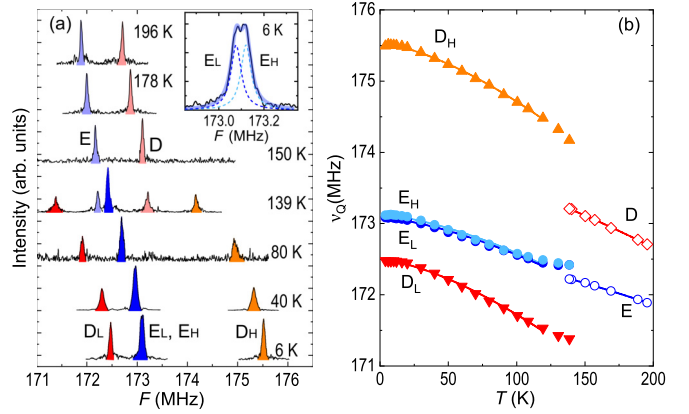
the ^{127}I nucleus [$-680(10)$ mb [43]], and Planck's constant, respectively.

In α-ET$_2$I$_3$, two crystallographically independent I$_3$ anions, D and E, exist [Fig. 1(c)]. Since the central iodine of each anion is located at the inversion center (1c and 1d sites in Wyckoff positions), the terminal iodines of each anion group are equivalent and occupied at 2i sites above T_{CO}. As a result, two independent terminal iodines exist, holding relations I1 = I3 and I2 = I4 ("=" denotes the site equivalency), which agrees with the two distinct lines observed in our NQR spectra. As discussed below, the signals at the high and low frequencies can be assigned to the D and E sites, respectively, from the calculation of the EFG using first-principles method.

At 139 K, five distinct lines are observed, as shown in Fig. 2(a), and the three lines remain at the lowest temperature. The temperature of 139 K corresponds to T_{CO}, and the co-existence of high-temperature and low-temperature peaks in the spectrum indicates that the phase transition is a first-order transition. Below T_{CO}, four lines are expected according to the loss of the inversion center by the CO transition [17]. Although the number of observed lines below T_{CO} is three, the intensities are approximately 1:2:1 from the low-frequency side, suggesting that the NQR spectra consist of four lines. The central peak below T_{CO} splits slightly, as shown in the inset of Fig. 2(a). We considered that two lines nearly overlap at $\nu_Q \approx 173$ MHz because they exhibit nearly the same magnitude of EFG at the terminal iodine sites.

All the ν_Q's increase upon cooling as a result of lattice contraction, as shown in Fig. 2(b). The slope of ν_Q at the D site is larger than that at the E site above T_{CO}, and below T_{CO}, the slopes of ν_Q at the high- and low-frequency signals are larger than that at the central frequency. An empirical formula for temperature-dependent $\nu_Q(T)$ considering thermal expansion of the unit cell [44],

$$\nu_Q(T) = \nu_0(1 - \alpha T^{3/2}), \quad (2)$$

fits the experiments well [solid lines in Fig. 2(b)], and we summarize the fitted parameters in Table I. Comparing α values, α at the D site is 1.5 times larger than at the E site above T_{CO}, and α at the two outer lines is also 1.5 times

TABLE I. Fitted parameters obtained by fitting $\nu_Q(T)$ at each site with Eq. (2)

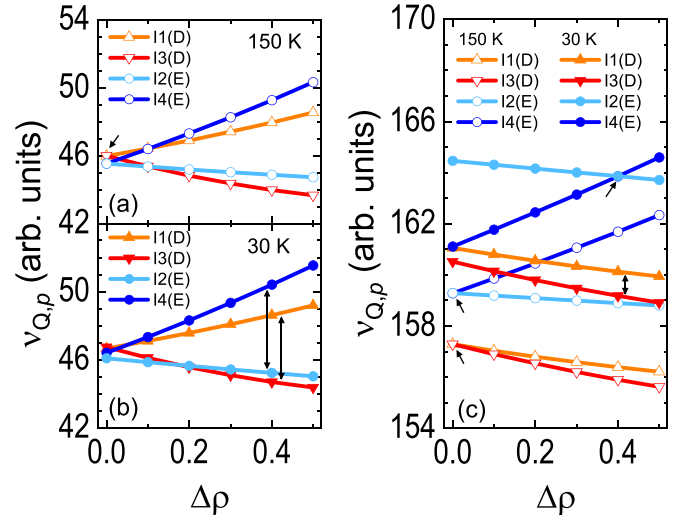|		ν_0 (MHz)	α (K$^{-3/2}$)
	$T > T_{CO}$	173.94(1)	2.61(4)
D	$T > T_{CO}$	172.493(6)	4.47(6)
		175.528(4)	4.64(4)
	$T > T_{CO}$	172.72(1)	1.76(3)
E	$T > T_{CO}$	173.081(7)	3.00(6)
		173.123(9)	3.09(9)

FIG. 3. (a)–(c) $\nu_{Q,p}$ calculated by the point charge model as a function of $\Delta\rho$ with $\rho = 0.5 \pm \Delta\rho$ ($0 < \Delta\rho < 0.5$). (a) and (b) show the calculation results based on the 150 and 30 K structures, respectively, taking into account only the charge of the ET layers. (c) shows the results for 150 and 30 K calculated by incorporating the charge of the I$_3$ layers in addition to the ET layers.

larger than at the central line below T_{CO}. The α value that is dependent on the iodine site can be attributed to the distinct principal axes of the EFG at D and E, relative to that of the thermal expansion. We concluded that the two outer lines originate from the D anion (hereafter, we refer to them as D$_H$ and D$_L$), and the overlapped central line originates from the E anion (E$_H$ and E$_L$). These results show that ν_Q of the D site changes significantly because of the CO transition, whereas the change in ν_Q of the E site is negligible. We calculated the EFG at each iodine position using the FLAPW method to clarify the relationship between the measured NQR signals and the actual iodine positions [35]. Since the EFG is usually very sensitive to internal atomic coordinates [45] and hydrogen atom positions determined from x-ray diffraction were not so accurate [46], we performed structural optimization for iodine and hydrogen atom positions. The relaxed structures with the crystallographic information file format and detailed calculation method are included in the Supplemental Material [35]. The calculated NQR frequencies ν_Q's are summarized in Table II along with the experimental values. At 150 K, the calculations show that $\nu_Q = 174.0$ MHz at the D site, which is 0.4% larger than $\nu_Q = 173.3$ MHz at the E site. Experimentally, the difference in frequency between the two NQR lines is approximately 0.5%, which is in good quantitative agreement. Hence, the high- and low-frequency lines are interpreted as signals originating from D and E anions.

At 30 K, the calculated ν_Q at the D site splits significantly into two lines with higher and lower frequencies, while the change at the E site is small. To discuss the amount of change in the D and E sites during the CO transition, we define

$$\left(\frac{\Delta\nu}{\nu}\right)_{Q,k} \equiv \frac{(\nu_{Q,k_H} - \nu_{Q,k_L})_{30\,K}}{(\nu_{Q,k})_{150\,K}}. \quad (3)$$

where $k = D, E$ sites, resulting in experimental values: $(\Delta\nu/\nu)_{Q,D} = 1.75\%$ and $(\Delta\nu/\nu)_{Q,E} = 0.02\%$; calculated

values: $(\Delta\nu/\nu)_{Q,D} = 0.74\%$ and $(\Delta\nu/\nu)_{Q,E} = 0.19\%$. The first-principles DFT calculations show that $(\Delta\nu/\nu)_{Q,D}$ is larger than $(\Delta\nu/\nu)_{Q,E}$, which qualitatively explain the experimental results, although ν_Q at the E site still split in the calculations.

In order to explore the cause behind the different conduct of the D and E sites, we performed calculations on the EFG that governs ν_Q, as a function of the charge-disproportionation ratio in the ET layer, by utilizing the point charge model (see the Supplemental Material [35]) [47,48]. Figures 3(a) and 3(b) show $\nu_{Q,p}$ ($p = $ I1–I4) only from the ET layers at 150 K [Fig. 3(a)] and 30 K [Fig. 3(b)] as a function of $\Delta\rho$ with $\rho = 0.5 \pm \Delta\rho$ ($0 < \Delta\rho < 0.5$). Here, the positive sign represents rich charge densities ρ for molecules A and B, while the negative sign corresponds to ρ for molecules A$'$ and C in the CO state. $\Delta\rho = 0$ is at a high-temperature electronic state, and $\Delta\rho = 0.2$–0.3 is reported in the CO state. At 150 K, because of $\Delta\rho = 0$ and the existence of the inversion symmetry, $\nu_{Q,I1}$ and $\nu_{Q,I3}$ ($\nu_{Q,I2}$ and $\nu_{Q,I4}$) must agree. The agreement of them at $\Delta\rho = 0$, indicated by the arrow [Fig. 3(a)], shows the validity of the calculation. There is no clear difference when we compare the ν_Q at 150 and 30 K. Moreover, as $\Delta\rho$ increases, the difference within each anion, i.e., $\nu_{Q,I1} - \nu_{Q,I3}$, $\nu_{Q,I2} - \nu_{Q,I4}$, increases [two-headed arrows in Fig. 3(b)]. This is inconsistent with the experimental results, in which the E

TABLE II. NQR frequencies of experiments (ν_Q^{exp}) and calculation (ν_Q^{cal}) for terminal iodines of I$_3$ anions.

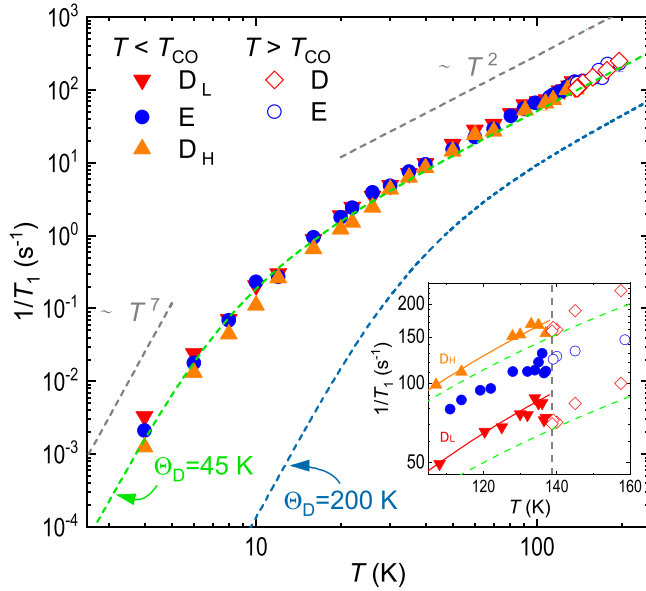|	D			E		
	ν_Q^{exp}(MHz)	ν_Q^{cal}(MHz)	Site	ν_Q^{exp}(MHz)	ν_Q^{cal}(MHz)	Site
150 K ($T > T_{CO}$)	173.10	174.0	I1(=I3)	172.17	173.3	I2(=I4)
30 K ($T < T_{CO}$)	175.40	175.2	I1	173.04	172.9	I2
	172.38	173.8	I3	173.00	172.6	I4

FIG. 4. Temperature dependence of $1/T_1$. The dashed lines are calculated $(1/T_1)_Q$ with $\Theta = 45$ and 200 K. The inset shows the temperature dependence of $1/T_1$ in the vicinity of T_{CO}. For clarity, the D_H and D_L data are multiplied and divided by 1.5, respectively. The solid curves are $1/T_1 = (1/T_1)_Q + \text{const} \times \exp(-\Delta/k_B T)$.

line hardly changes in the temperature-dependent spectra and the D line changes significantly.

Next, we computed the EFG incorporating the EFG from the negative charges of the I_3 layers and show $\nu_{Q,p}$ in Fig. 3(c). The magnitudes of the change in $\nu_{Q,I2}$ and $\nu_{Q,I4}$ across the CO transition differ significantly: $\nu_{Q,I2} - \nu_{Q,I4} = 0$ at $\Delta\rho = 0$ for 150 K, and that at $\Delta\rho = 0.4$ for 30 K. On the other hand, $\nu_{Q,I1} - \nu_{Q,I3}$ is minimized at $\Delta\rho = 0$ both for 150 and 30 K, and $\nu_{Q,I1} - \nu_{Q,I3}$ at all $\Delta\rho$ for 30 K is greater than zero. The less pronounced differentiation in ν_Q at the E site compared to the D site in the CO state is replicated, indicating the substantial role of the interaction between the anion and cation in reproducing the microscopic spectroscopy.

As the origin of this anion-cation interaction, Alemany *et al.* [34] pointed out that the hydrogen bonding is important and that the E anion is more strongly bound to hydrogen atoms than the D anion. The presence of hydrogen bonding would enhance the anion-cation interaction. The observed larger change in ν_Q at the E site is consistent with this argument. Hydrogen bonding has been discussed experimentally from a structural analysis [34] and also by transport measurements [49]. In this study, we were able to explore the hydrogen bonding from a microscopic point of view.

B. Relaxation rate

In Fig. 4, we show the temperature-dependent nuclear spin-lattice relaxation rate $1/T_1$ for each spectral line. No significant variation in $1/T_1$ for the distinct lines is observed. The $1/T_1$ nearly follows power relations in regards to temperature, $1/T_1 \propto T^\beta$, which differs from ^{13}C NMR [24]. The β changes from high temperature, $\beta = 2$, to low temperature, $\beta \approx 7$, suggesting that the relaxation mechanism is quadrupolar relaxation of nuclei by two-phonon Raman processes

[50,51]. The $1/T_1$ originating from this process is expressed as [52]

$$\left(\frac{1}{T_1}\right)_Q \simeq \frac{81\pi}{2}\left(\frac{F_2\hbar}{mv^2}\right)^2 \int_0^\Omega \frac{e^{\hbar\omega/k_B T}}{(e^{\hbar\omega/k_B T}-1)^2}\left(\frac{\omega}{\Omega}\right)^6 d\omega, \quad (4)$$

where k_B, m, Ω are the Boltzmann constant, the mass of the ^{127}I nucleus, and a cutoff frequency, respectively. v is the sound velocity in the crystal, which is an order of 10^3 m/s in organic conductors [53]. Ω is represented by the temperature $\Theta = (\hbar/k_B)\Omega$ and can be estimated as the Debye temperature, $\Theta = \Theta_D = 200$ K, which is obtained by heat capacity measurements of ET organic conductors. F_2 characterizes the phonon modulation of the EFG and is difficult to determine precisely; however, the simplest estimate, $F_2 = 2\pi\nu_Q$, works well [51,54].

The calculated $(1/T_1)_Q$ is plotted as the blue dashed line in Fig. 4 using $\nu_Q = 173$ MHz and $\Theta = 200$ K, which is significantly smaller than the experimental $1/T_1$. Instead, the calculated $(1/T_1)_Q$ using $\Theta = 45$ K (green dashed line) reproduces the experiments well. This discrepancy suggests that the local Θ at iodine sites in Eq. (4) can be smaller than the global Debye temperature Θ_D estimated from macroscopic measurements. We can cite several related experiments. The ^{129}I-Mössbauer results of β-ET$_2$I$_3$ have been explained using the local Debye temperature of $\sim$100 K [55], which is smaller than $\Theta_D \simeq 200$ K estimated from the heat capacity measurement [56]. Raman spectra also showed a low-lying molecular vibration mode with 27 cm^{-1} ($= 38$ K) assigned to the libration of I$_3$ anions, a reciprocating motion with a fixed position in the middle of the I$_3$ "stick" (i.e., the central iodine). These arguments are consistent with our observations.

Around the T_{CO}, we found small peaks for $1/T_1$ of the charge-sensitive D_H and D_L lines, as shown in the inset of Fig. 4. Notably, that the peak temperature is located just below T_{CO}, by which we consider the source for the additional relaxation is not a critical slowing down for the CO. A similar peak for $1/T_1$ just below the T_{CO} was observed by ^{13}C-NMR for the charge-rich site [24]. Reference [24] argues that an emergent antiferromagnetic zigzag chain ($S = 1/2$) for $T < T_{CO}$ undergoes a singlet state with a sizable gap of $\Delta = 40$ meV [29]. We plot $1/T_1 = (1/T_1)_Q + \text{const} \times \exp(-\Delta/k_B T)$ as the solid lines in the inset of Fig. 4 and find good agreements with the experimental $1/T_1$ for the D_H and D_L sites. However, we cannot conclude that magnetic fluctuation from charge-ordered ET layers is the source for the peaks of $1/T_1$ because $1/T_1$ for D_H and D_L sites that are close to charge-rich and charge-poor ET molecules show comparable enhancements.

When we consider the difference in the relaxation mechanisms of ^{13}C and ^{127}I (i.e., magnetic fluctuation of the local spin density for the former and EFG fluctuation for the latter), we can point out another possibility, other than an emergent spin chain that undergoes a spin-singlet state. In charge-density-wave (CDW) systems, it is argued that coherence peaklike properties just below the transition temperature can emerge, originating from singularity of the density of states across the CDW gap [57–59]. The electron density is also expected to follow an activated T dependence; then, we cannot discriminate between the energy gaps in the CDW and spin-singlet Mott systems. The first-principles calculations

also show a similar singularity for the gap opening due to Coulomb repulsion [60,61]. Detailed theoretical analyses considering the gap structures and the relationships between the magnitudes of the gap and leading electronic/magnetic interactions are necessary to determine the origins of the gap.

In summary, we obtained ^{127}I-NQR spectra and $1/T_1$ for α-ET$_2$I$_3$ that undergoes a CO transition at ambient pressure. The first-principles calculations accurately reproduced the NQR frequency of each spectral line, which enabled us to examine the microscopic interactions. The spectral line at the D site splits significantly, while that at the E site is negligibly small. These results are qualitatively reproduced by EFG calculations based on a point-charge model that incorporates contributions from both ET and I$_3$ layers, suggesting the importance of the anion-cation interaction. Furthermore, $1/T_1$ is predominantly determined by a two-phonon process characterized by the local vibration of I$_3$ anions. The charge-order phase transition is first order, without a critical slowing down of the electronic charges. Just below the T_{CO}, $1/T_1$ shows an additional relaxation similar to the reported ^{13}C NMR.

[1] H. Seo, Charge ordering in organic ET compounds, J. Phys. Soc. Jpn. **69**, 805 (2000).

[2] K. Miyagawa, A. Kawamoto, and K. Kanoda, Charge ordering in a quasi-two-dimensional organic conductor, Phys. Rev. B **62**, R7679 (2000).

[3] K. Yamamoto, S. Iwai, S. Boyko, A. Kashiwazaki, F. Hiramatsu, C. Okabe, N. Nishi, and K. Yakushi, Strong optical nonlinearity and its ultrafast response associated with electron ferroelectricity in an organic conductor, J. Phys. Soc. Jpn. **77**, 074709 (2008).

[4] S. Tomić and M. Dressel, Ferroelectricity in molecular solids: a review of electrodynamic properties, Rep. Prog. Phys. **78**, 096501 (2015).

[5] F. Kagawa, T. Sato, K. Miyagawa, K. Kanoda, Y. Tokura, K. Kobayashi, R. Kumai, and Y. Murakami, Charge-cluster glass in an organic conductor, Nat. Phys. **9**, 419 (2013).

[6] H. Mori, S. Tanaka, and T. Mori, Systematic study of the electronic state in θ-type BEDT-TTF organic conductors by changing the electronic correlation, Phys. Rev. B **57**, 12023 (1998).

[7] J. Merino and R. H. McKenzie, Superconductivity Mediated by Charge Fluctuations in Layered Molecular Crystals, Phys. Rev. Lett. **87**, 237002 (2001).

[8] A. F. Bangura, A. I. Coldea, J. Singleton, A. Ardavan, A. Akutsu-Sato, H. Akutsu, S. S. Turner, P. Day, T. Yamamoto, and K. Yakushi, Robust superconducting state in the low-quasiparticle-density organic metals β''-(BEDT-TTF)$_4$[(H$_3$O)M(C$_2$O$_4$)$_3$] $\cdot$ Y: Superconductivity due to proximity to a charge-ordered state, Phys. Rev. B **72**, 014543 (2005).

[9] A. Pustogow, K. Treptow, A. Rohwer, Y. Saito, M. Sanz Alonso, A. Löhle, J. A. Schlueter, and M. Dressel, Charge order in β''-phase BEDT-TTF salts, Phys. Rev. B **99**, 155144 (2019).

[10] M. Dressel and S. Tomić, Molecular quantum materials: electronic phases and charge dynamics in two-dimensional organic solids, Adv. Phys. **69**, 1 (2020).

[11] N. Tajima, M. Tamura, Y. Nishio, K. Kajita, and Y. Iye, Transport property of an organic conductor α-(BEDT-TTF)$_2$I$_3$ under high pressure: Discovery of a novel type of conductor, J. Phys. Soc. Jpn. **69**, 543 (2000).

[12] S. Katayama, A. Kobayashi, and Y. Suzumura, Pressure-induced zero-gap semiconducting state in organic conductor α-(BEDT-TTF)$_2$I$_3$ salt, J. Phys. Soc. Jpn. **75**, 054705 (2006).

[13] K. Kajita, Y. Nishio, N. Tajima, Y. Suzumura, and A. Kobayashi, Molecular Dirac fermion systems: Theoretical and experimental approaches, J. Phys. Soc. Jpn. **83**, 072002 (2014).

[14] M. Hirata, K. Ishikawa, G. Matsuno, A. Kobayashi, K. Miyagawa, M. Tamura, C. Berthier, and K. Kanoda, Anomalous spin correlations and excitonic instability of interacting 2D Weyl fermions, Science **358**, 1403 (2017).

[15] S. Fujiyama, H. Maebashi, N. Tajima, T. Tsumuraya, H.-B. Cui, M. Ogata, and R. Kato, Large Diamagnetism and Electromagnetic Duality in Two-Dimensional Dirac Electron System, Phys. Rev. Lett. **128**, 027201 (2022).

[16] K. Bender, I. Hennig, D. Schweitzer, K. Dietz, H. Endres, and H. J. Keller, Synthesis, structure and physical properties of a two-dimensional organic metal, Di[bis(ethylenedithiolo) tetrathiofulvalene] triiodide, (BEDT-TTF)$_2$$^+I_3$$^-$, Mol. Cryst. Liq. Cryst. **108**, 359 (1984).

[17] T. Kakiuchi, Y. Wakabayashi, H. Sawa, T. Takahashi, and T. Nakamura, Charge ordering in α-(BEDT-TTF)$_2$I$_3$ by synchrotron x-ray diffraction, J. Phys. Soc. Jpn. **76**, 113702 (2007).

[18] R. Wojciechowski, K. Yamamoto, K. Yakushi, M. Inokuchi, and A. Kawamoto, High-pressure Raman study of the charge ordering in α-(BEDT-TTF)$_2$I$_3$, Phys. Rev. B **67**, 224105 (2003).

[19] T. Ivek, B. Korin-Hamzić, O. Milat, S. Tomić, C. Clauss, N. Drichko, D. Schweitzer, and M. Dressel, Electrodynamic response of the charge ordering phase: Dielectric and optical studies of α-(BEDT-TTF)$_2$I$_3$, Phys. Rev. B **83**, 165128 (2011).

[20] K. Yakushi, Infrared and Raman studies of charge ordering in organic conductors, BEDT-TTF salts with quarter-filled bands, Crystals **2**, 1291 (2012).

[21] Y. Takano, K. Hiraki, H. M. Yamamoto, T. Nakamura, and T. Takahashi, Charge disproportionation in the organic conductor, α-(BEDT-TTF)$_2$I$_3$, J. Phys. Chem. Solids **62**, 393 (2001).

[22] S. Hirose and A. Kawamoto, Local spin susceptibility in the zero-gap-semiconductor state of α-(BEDT-TTF)$_2$I$_3$ probed by ^{13}C NMR under pressure, Phys. Rev. B **82**, 115114 (2010).

[23] M. Hirata, K. Ishikawa, K. Miyagawa, K. Kanoda, and M. Tamura, ^{13}C NMR study on the charge-disproportionated conducting state in the quasi-two-dimensional organic conductor α-(BEDT-TTF)$_2$I$_3$, Phys. Rev. B **84**, 125133 (2011).

[24] K. Ishikawa, M. Hirata, D. Liu, K. Miyagawa, M. Tamura, and K. Kanoda, Spin excitations in the quasi-two-dimensional charge-ordered insulator α-(BEDT-TTF)$_2$I$_3$ probed via ^{13}C NMR, Phys. Rev. B **94**, 085154 (2016).

[25] S. Kitou, T. Tsumuraya, H. Sawahata, F. Ishii, K.-i. Hiraki, T. Nakamura, N. Katayama, and H. Sawa, Ambient-pressure Dirac electron system in the quasi-two-dimensional molecular conductor α-(BETS)$_2$I$_3$, Phys. Rev. B **103**, 035135 (2021).

[26] H. Kino and H. Fukuyama, On the phase transition of α-(ET)$_2$I$_3$, J. Phys. Soc. Jpn. **64**, 1877 (1995).

[27] H. Kino and H. Fukuyama, Phase diagram of two-dimensional organic conductors: (BEDT-TTF)$_2$X, J. Phys. Soc. Jpn. **65**, 2158 (1996).

[28] H. Seo and H. Fukuyama, Antiferromagnetic phases of one-dimensional quarter-filled organic conductors, J. Phys. Soc. Jpn. **66**, 1249 (1997).

[29] Y. Tanaka and M. Ogata, Correlation effects on charge order and zero-gap state in the organic conductor α-(BEDT-TTF)$_2$X, J. Phys. Soc. Jpn. **85**, 104706 (2016).

[30] R. Torsten Clay, S. Mazumdar, and D. K. Campbell, Charge ordering in θ-(BEDT-TTF)$_2$X materials, J. Phys. Soc. Jpn. **71**, 1816 (2002).

[31] Y. Tanaka and K. Yonemitsu, Charge order with structural distortion in organic conductors: Comparison between θ-(ET)$_2$RbZn(SCN)$_4$ and α-(ET)$_2$I$_3$, J. Phys. Soc. Jpn. **77**, 034708 (2008).

[32] S. Miyashita, Y. Tanaka, S. Iwai, and K. Yonemitsu, Charge, lattice, and spin dynamics in photoinduced phase transitions from charge-ordered insulator to metal in quasi-two-dimensional organic conductors, J. Phys. Soc. Jpn. **79**, 034708 (2010).

[33] M. Udagawa and Y. Motome, Charge Ordering and Coexistence of Charge Fluctuations in Quasi-Two-Dimensional Organic Conductors θ-(BEDT-TTF)$_2$X, Phys. Rev. Lett. **98**, 206405 (2007).

[34] P. Alemany, J.-P. Pouget, and E. Canadell, Essential role of anions in the charge ordering transition of α-(BEDT-TTF)$_2$I$_3$, Phys. Rev. B **85**, 195118 (2012).

[35] See Supplemental Material at http://link.aps.org/supplemental/10.1103/PhysRevB.108.115108 for the detailed calculation of EFG and relaxation curves.

[36] D. E. MacLaughlin, J. D. Williamson, and J. Butterworth, Nuclear spin-lattice relaxation in pure and impure indium. i. normal state, Phys. Rev. B **4**, 60 (1971).

[37] A. C. Daniel and W. G. Moulton, Temperature dependence of pure nuclear quadrupole spin-lattice relaxation in SnI$_4$, J. Chem. Phys. **41**, 1833 (1964).

[38] E. Wimmer, H. Krakauer, M. Weinert, and A. J. Freeman, Full-potential self-consistent linearized-augmented-plane-wave method for calculating the electronic structure of molecules and surfaces: O$_2$ molecule, Phys. Rev. B **24**, 864 (1981).

[39] J. Yu, A. J. Freeman, R. Podloucky, P. Herzig, and P. Weinberger, Origin of electric-field gradients in high-temperature superconductors: YBa$_2$Cu$_3$O$_7$, Phys. Rev. B **43**, 532 (1991).

[40] J. P. Perdew, K. Burke, and M. Ernzerhof, Generalized Gradient Approximation Made Simple, Phys. Rev. Lett. **77**, 3865 (1996).

[41] Y. Yoshioka, N. Nakamura, and H. Chihara, On the correlation between NQR frequency and bond length in I$_3$$^-$, J. Mol. Struct. **111**, 151 (1983).

[42] G. A. Bowmaker and S. Hacobian, Nuclear quadrupole resonance of charge transfer complexes. I. The trihalide ions, Aust. J. Chem. **21**, 551 (1968).

[43] H. Yakobi, E. Eliav, L. Visscher, and U. Kaldor, High-accuracy calculation of nuclear quadrupole moments of atomic halogens, J. Chem. Phys. **126**, 054301 (2007).

[44] J. Christiansen, P. Heubes, R. Keitel, W. Klinger, W. Loeffler, W. Sandner, and W. Witthuhn, Temperature dependence of the electric field gradient in noncubic metals, Z. Phys. B **24**, 177 (1976).

[45] P. Blaha, D. J. Singh, P. I. Sorantin, and K. Schwarz, Electric-field-gradient calculations for systems with large extended-core-state contributions, Phys. Rev. B **46**, 1321 (1992).

[46] P. T. Edwards, L. K. Saunders, D. C. Grinter, P. Ferrer, G. Held, E. J. Shotton, and S. L. M. Schroeder, Determination of H-atom positions in organic crystal structures by nexafs combined with density functional theory: a study of two-component systems containing isonicotinamide, J. Phys. Chem. A **126**, 2889 (2022).

[47] W. Gabes and M. A. M. Nijman-Meester, Semiempirical molecular orbital calculation of symmetrical trihalide ions, Inorg. Chem. **12**, 589 (1973).

[48] T. Mori, A. Kobayashi, Y. Sasaki, H. Kobayashi, G. Saito, and H. Inokuchi, The intermolecular interaction of tetrathiafulvalene and bis(ethylenedithio)tetrathiafulvalene in organic metals. Calculation of orbital overlaps and models of energy-band structures, Bull. Chem. Soc. Jpn. **57**, 627 (1984).

[49] T. Ivek, M. Čulo, M. Kuveždić, E. Tutiš, M. Basletić, B. Mihaljević, E. Tafra, S. Tomić, A. Löhle, M. Dressel, D. Schweitzer, and B. Korin-Hamzić, Semimetallic and charge-ordered α-(BEDT-TTF)$_2$I$_3$: On the role of disorder in dc transport and dielectric properties, Phys. Rev. B **96**, 075141 (2017).

[50] F. Iwase, K. Miyagawa, S. Fujiyama, K. Kanoda, S. Horiuchi, and Y. Tokura, Neutral-ionic phase transition in DMTTF-QCl$_4$ investigated by ^{35}Cl NQR, J. Phys. Soc. Jpn. **76**, 073701 (2007).

[51] T. Kobayashi, Q.-P. Ding, H. Taniguchi, K. Satoh, A. Kawamoto, and Y. Furukawa, Charge disproportionation in the spin-liquid candidate κ-(ET)$_2$Cu$_2$(CN)$_3$ at 6 K revealed by ^{63}Cu NQR measurements, Phys. Rev. Res. **2**, 042023(R) (2020).

[52] A. A. Abragam, *The Principles of Nuclear Magnetism* (Oxford University Press, Oxford, UK, 1961).

[53] S. Imajo (private communication).

[54] M. Klanjšek, A. Zorko, R. Žitko, J. Mravlje, Z. Jagličić, P. K. Biswas, P. Prelovšek, D. Mihailovic, and D. Arčon, A high-temperature quantum spin liquid with polaron spins, Nat. Phys. **13**, 1130 (2017).

[55] G. Wortmann, E. Bychkov, and Y. S. Grushko, ^{129}I-Mössbauer study of molecular dynamics in the organic superconductor β-(BEDT-TTF)$_2$I$_3$, Hyperfine Interact. **70**, 1179 (1992).

[56] G. R. Stewart, J. O'Rourke, G. W. Crabtree, K. D. Carlson, H. H. Wang, J. M. Williams, F. Gross, and K. Andres, Specific heat of the ambient-pressure organic superconductor β-di[bis(ethylenedithio)tetrathiafulvalene] triiodide [β-(BEDT-TTF)$_2$I$_3$], Phys. Rev. B **33**, 2046 (1986).

[57] G. Grüner, The dynamics of charge-density waves, Rev. Mod. Phys. **60**, 1129 (1988).

[58] P. Matus, P. Bánki, and G. Kriza, ^{87}Rb NMR spin-lattice relaxation in the charge-density wave phase of Rb$_{0.3}$MoO$_3$, J. Phys. IV **09**, Pr10-267 (1999).

[59] T. Maniv, Effect of a spin density wave instability on the nuclear spin-lattice relaxation in quasi 1-d conductors, Solid State Commun. **43**, 47 (1982).

[60] T. Tsumuraya, H. Seo, and T. Miyazaki, First-principles study of charge ordered phase in κ-D$_3$(Cat-EDT-TTF/ST)$_2$: Stability

of π-electron-deuterium coupled ordering in hydrogen-bonded molecular conductors, Phys. Rev. B **101**, 045114 (2020).

[61] T. Tsumuraya, H. Seo, and T. Miyazaki, First-principles study on the stability and electronic structure of the charge-ordered phase in α-(BEDT-TTF)$_2$I$_3$, Crystals **11**, 1109 (2021).